

# Constraints on WIMP-like dark matter scattering on electrons with COSINE-100

N. Carlin,<sup>1</sup> J. Y. Cho,<sup>2</sup> S. J. Cho,<sup>3</sup> S. Choi,<sup>4</sup> A. C. Ezeribe,<sup>5</sup> L. E. França,<sup>1,\*</sup> O. Gileva,<sup>3</sup> C. Ha,<sup>6</sup> I. S. Hahn,<sup>7,8,9</sup> S. J. Hollick,<sup>10</sup> E. J. Jeon,<sup>3,9</sup> H. W. Joo,<sup>4</sup> W. G. Kang,<sup>3</sup> M. Kauer,<sup>11</sup> B. H. Kim,<sup>3</sup> D. Y. Kim,<sup>3</sup> H. J. Kim,<sup>2</sup> J. Kim,<sup>6</sup> K. W. Kim,<sup>3</sup> S. H. Kim,<sup>3</sup> S. K. Kim,<sup>4</sup> W. K. Kim,<sup>9,3</sup> Y. D. Kim,<sup>3,9</sup> Y. H. Kim,<sup>3,9</sup> B. R. Ko,<sup>12</sup> Y. J. Ko,<sup>13</sup> D. H. Lee,<sup>2</sup> E. K. Lee,<sup>3</sup> H. Lee,<sup>9,3</sup> H. S. Lee,<sup>3,9</sup> H. Y. Lee,<sup>7</sup> I. S. Lee,<sup>3</sup> J. Lee,<sup>3</sup> J. Y. Lee,<sup>2</sup> M. H. Lee,<sup>3,9</sup> S. H. Lee,<sup>9,3</sup> S. M. Lee,<sup>4</sup> Y. J. Lee,<sup>6</sup> D. S. Leonard,<sup>3</sup> N. T. Luan,<sup>2</sup> V. H. A. Machado,<sup>1</sup> B. B. Manzato,<sup>1</sup> R. H. Maruyama,<sup>10</sup> S. L. Olsen,<sup>3</sup> H. K. Park,<sup>12</sup> H. S. Park,<sup>14</sup> J. C. Park,<sup>15</sup> J. S. Park,<sup>2</sup> K. S. Park,<sup>3</sup> K. Park,<sup>3</sup> S. D. Park,<sup>2</sup> R. L. C. Pitta,<sup>1</sup> H. Prihtiadi,<sup>16</sup> S. J. Ra,<sup>3</sup> C. Rott,<sup>17</sup> K. A. Shin,<sup>3</sup> D. F. F. S. Cavalcante,<sup>1</sup> M. K. Son,<sup>15</sup> N. J. C. Spooner,<sup>5</sup> L. T. Truc,<sup>2</sup> L. Yang,<sup>18</sup> and G. H. Yu<sup>3</sup>  
(COSINE-100 Collaboration)

<sup>1</sup>*Physics Institute, University of São Paulo, 05508-090, São Paulo, Brazil*

<sup>2</sup>*Department of Physics, Kyungpook National University, Daegu 41566, Republic of Korea*

<sup>3</sup>*Center for Underground Physics, Institute for Basic Science (IBS), Daejeon 34126, Republic of Korea*

<sup>4</sup>*Department of Physics and Astronomy, Seoul National University, Seoul 08826, Republic of Korea*

<sup>5</sup>*Department of Physics and Astronomy, University of Sheffield, Sheffield S3 7RH, United Kingdom*

<sup>6</sup>*Department of Physics, Chung-Ang University, Seoul 06973, Republic of Korea*

<sup>7</sup>*Center for Exotic Nuclear Studies, Institute for Basic Science (IBS), Daejeon 34126, Republic of Korea*

<sup>8</sup>*Department of Science Education, Ewha Womans University, Seoul 03760, Republic of Korea*

<sup>9</sup>*IBS School, University of Science and Technology (UST), Daejeon 34113, Republic of Korea*

<sup>10</sup>*Department of Physics and Wright Laboratory, Yale University, New Haven, CT 06520, USA*

<sup>11</sup>*Department of Physics and Wisconsin IceCube Particle Astrophysics Center, University of Wisconsin-Madison, Madison, WI 53706, USA*

<sup>12</sup>*Department of Accelerator Science, Korea University, Sejong 30019, Republic of Korea*

<sup>13</sup>*Department of Physics, Jeju National University, Jeju 63243, Republic of Korea*

<sup>14</sup>*Korea Research Institute of Standards and Science, Daejeon 34113, Republic of Korea*

<sup>15</sup>*Department of Physics and Institute for Sciences of the Universe, Chungnam National University, Daejeon 34134, Republic of Korea*

<sup>16</sup>*Department of Physics, Universitas Negeri Malang, Malang 65145, Indonesia*

<sup>17</sup>*Department of Physics and Astronomy, University of Utah, Salt Lake City, UT 84112, USA*

<sup>18</sup>*Department of Physics, University of California San Diego, La Jolla, CA 92093, USA*

(Dated: October 6, 2025)

We present results of the search for WIMP-like dark matter interaction with electrons in the NaI(Tl) crystals of the COSINE-100 experiment. The two benchmark scenarios of a heavy and a light vector boson as mediator of the interaction were studied. We found no excess events over the expected background in a data-set of 2.82 years, with a total exposure of 172.9 kg-year. The derived 90% confidence level upper limits exclude a WIMP-electron scattering cross section above  $6.4 \times 10^{-33} \text{ cm}^2$  for a WIMP mass of 0.25 GeV, assuming a light mediator; and above  $3.4 \times 10^{-37} \text{ cm}^2$  for a 0.4 GeV WIMP, assuming a heavy mediator, and represent the most stringent constraints for a NaI(Tl) target to date. We also briefly discuss a planned analysis using an annual modulation method below the current 0.7 keV threshold of COSINE-100, down to few photoelectrons yield.

## I. INTRODUCTION

The existence of cold dark matter (CDM) is supported by numerous astrophysical and cosmological observations that demonstrate its gravitational interactions. All evidence is compatible with 85% of the matter in the universe being composed of DM. Nevertheless, the precise nature of DM particles remains unknown, prompting extensive research in the field of particle physics [1–5]. One of the main DM candidates is the Weakly Interacting Massive Particle (WIMP). Due to the WIMP miracle [6] and since different theories that extend the standard model propose particles with the WIMP properties,

WIMPs are rendered as a highly promising candidate [7].

To date, the most studied scenario considers a weak interaction between WIMPs and nucleons. Nonetheless, because there is no compelling evidence of WIMP detection in the results from multiple direct detection experiments utilizing different detector materials, as well as the increasingly stringent constraints on the WIMP-nucleon cross section and WIMP mass [8–11], studies of alternative models are encouraged [12–15]. One such alternative involves interactions between WIMP-like cold DM and electrons [16], which could be detected in modern low threshold detectors. This is particularly relevant in the context of sub-GeV WIMPs, where increased sensitivity to this interaction is anticipated. Given that the largest unexplored region pertains to sub-GeV WIMPs, the WIMP-electron scattering is a viable and appropriate

\* [luis.eduardo.franca@usp.br](mailto:luis.eduardo.franca@usp.br)

scenario.

Several collaborations have reported their searches for the WIMP-electron interaction, constraining its cross section [17–20]. As a consequence of the low threshold, silicon based experiments, such as DAMIC-M [21] and SENSEI [22], have set the most stringent limits for lighter WIMPs within the mass region of 1 to approximately 100 MeV. In contrast, as a result of the high detector exposure, liquid noble gas experiments, such as PANDAX-4T [23], DarkSide-50 [24] and XENONnT [25], have provided the strongest constraints for WIMPs with masses exceeding 100 MeV. Despite that, up to this moment, no experiment utilizing NaI(Tl) detectors has published a dedicated search for this cold DM WIMP-electron interaction model. The NEON experiment has recently published a search for light DM scattering on electrons in NaI(Tl) detectors [26], probing DM masses in the keV range. However, the studied model consisted in DM particles produced by the invisible decay of dark photons generated in the core of a nuclear reactor, which only enabled the search for DM masses up to 1 MeV. Some studies have interpreted the long-lasting DAMA/LIBRA modulation results [27, 28] in relation to the detection of WIMP scattering on electrons [29, 30]. These studies have determined the values for WIMP mass and cross section with electrons related to the best-fit to DAMA modulation data. While WIMP-electron scattering alone cannot fully account for the modulated signal across the entire DAMA/LIBRA energy spectrum, it has been proposed as a potential contributor, particularly in the low-energy region near 1 keV. Also, especially with the threshold reduction of DAMA/LIBRA’s crystals to 0.75 keV, this model can only partially explain DAMA’s modulation results, with good fitting near the 1 keV energy range, but poor accordance for energies up to 6 keV. However, due to the lack of searches for the WIMP-electron scattering model in NaI(Tl) detectors, investigating it with COSINE-100 can be highly useful for confirming and expanding the restrictions on the WIMP-electron cross section.

This work presents the results of the search for events generated by WIMP-like DM scattering on electrons in the COSINE-100 experiment. Excess events over the expected background were searched in a data-set of 2.82 years, using 61.3 kg of NaI(Tl), totalizing an exposure of 172.9 kg-year. A reduced analysis threshold of 8 photoelectrons, corresponding to an energy of 0.7 keV, has been achieved in COSINE-100 crystals [31], thereby significantly improving the sensitivity for the detection of light WIMPs scattering on electrons. The presented study addresses two traditional cases of the WIMP-electron scattering mediated by a vector boson: a mediator that is much heavier than the electron, resulting in a contact interaction, and a mediator much lighter than the electron, resulting in a long-range interaction.

This paper is structured as follows: in Section II, the COSINE-100 detector, data acquisition system, and operation are described. In Section III, the DM-electron

interaction model is detailed, with emphasis on the main relevant expressions for direct detection studies. A brief discussion about an accurate description of the NaI ionization factor appropriate to the energies involved in this analysis is also presented. In Section IV, the data analysis procedure is reported, describing data treatment and the detector performance at the region of interest (ROI), background components, expected spectra generated by the DM-electron scattering, signal fitting and the resulting constraints for COSINE-100. In Section V, prospects for a more sensitive analysis in COSINE-100 and in its upgraded version COSINE-100U are presented. Finally, a summary highlighting the main results and contributions of this work is provided in Section VI.

## II. COSINE-100 EXPERIMENT

The COSINE-100 experiment was installed at the *YangYang* underground laboratory in South Korea, and operated from September 22, 2016, to March 14, 2023. The shortest distance between the surface and the laboratory is 700 m. The main detectors were 8 NaI(Tl) ultrapure crystals, with a total of 106 kg, which were connected in each end to a Hamamatsu R12669SEL photomultiplier tube (PMT). Between the PMTs end faces and the crystals there were 12 mm quartz windows light guides. Oxygen free copper cases encapsulated the crystals, which were immersed in 2200 L of a liquid scintillator (LS) based on linear alkylbenzene, and positioned in a  $4 \times 2$  array on acrylic tables.

Active and passive vetoes were present in the COSINE-100 experiment. Surrounding the LS there were a 3 cm thick copper shield, low activity 20 cm thick lead bricks, and 37 Eljen EJ-200 plastic scintillator panels, present as an active veto for cosmic muons. The LS acts not only as a passive and active veto, but is also crucial for measuring the activity of radioisotopes contributing to the background in the crystals. Fig. 1 shows a schematic view of the COSINE-100 experiment.

Each PMT attached to the crystals had a dynode, whose signals are suitable for analyses with energies above 100 keV up to few MeVs, in which signals become saturated; and an anode, whose signals are used in low energy analyses, such as the one presented in this work. Even though all 8 crystals are used in analyses above 100 keV, 3 crystals have a poor performance for low energy signals due to low light yield and high noise and background rate. Hence, only data from the remaining 5 crystals are suitable for low energy analysis, and have been used in COSINE-100 WIMP searches [32, 33]. The total effective mass of these 5 crystals is 61.3 kg.

Anode signals from the crystals’ PMTs were amplified by a factor of 30 and dynode signals amplified by a factor of 100 before processed by 500 mega sample per second (MSPS) FADC modules. As for the active vetoes, signals were read by 63.5 MSPS analog to digital converter (M64ADC) modules. Signals from the plastic scintilla-

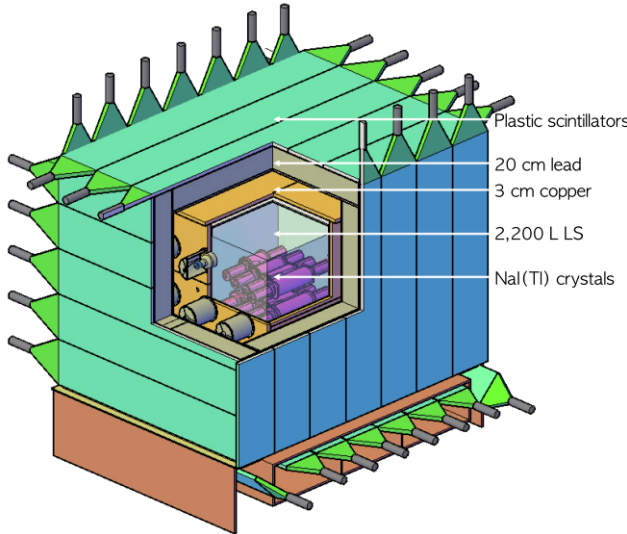


FIG. 1. Illustration of the COSINE-100 experiment. The NaI(Tl) crystals arrange, LS and plastic panels, and passive shields are presented.

tors and crystals were in the core of the trigger logic. If the pulse height of a signal in any crystal PMT rises above a threshold of 6 mV, a coincidence gate of 200 ns was generated waiting for another signal above threshold in the other PMT in the same crystal. When the coincidence was observed, the TCB created a global trigger and data from all FADC and M64ADC modules were stored. A global trigger could also be generated if two or more plastic panels observed coincident events. Hence, LS events could only be stored if signals from at least one crystal or two plastic panels were triggered.

Variables from the laboratory environment and detector stability parameters were monitored. Detectors event rate, behavior of parameters used for event selection, and other detector aspects related to its stability were daily monitored by the collaboration. Environment variables were also controlled through the Grafana application [34], as for example the PMTs voltage levels, relative humidity, radon air concentration and the detectors temperature. More details of the COSINE-100 experiment detectors performance, data acquisition system, and environmental monitoring are reported in Refs. [35–38].

### III. DM-ELECTRON SCATTERING MODEL

#### A. Overview and key expressions for direct detection

According to the momentum and energy conservations, WIMPs deposit more energy in the target when scattering on particles that have a mass similar to their own. Hence, the recent focus on searches for lighter WIMPs, especially below 10 GeV, has motivated the increase in the number of studies about WIMP-like DM interaction

with electrons in the last years, since light WIMPs, with mass below few GeVs, can induce a detectable amount of events above the threshold of current detectors.

Although the standard WIMP-nucleon scattering scenario assumes a weak interaction [39], there are no restrictions in the models to DM interacting simultaneously with nucleons and electrons, despite a new vector boson is commonly postulated in the latter framework [16]. The most frequently considered model for the interaction between WIMPs and electrons suggests a hidden sector boson to be the mediator, without restrictions to its spin and parity [29]. However, in order to simplify the model and accommodate the well motivated scenario of the dark photon [14], this boson is supposed to be a vector. In this work, we consider only the scattering between WIMPs and electrons, neglecting the WIMP-nucleon interaction, in order to directly compare the analysis with reported studies from other experiments. Nevertheless, the typical momentum transfer involved in the scattering is much smaller than the sodium and iodine nuclei masses, implying that the nuclear recoil energy would be negligible. In this scenario, the Feynman diagram representing the scattering is presented in Fig. 2.

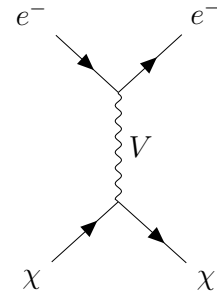


FIG. 2. Feynman diagram that represents the DM-electron scattering, where  $V$  is a vector boson and  $\chi$  is the WIMP.

Generally, describing the kinematics of the electron ionization by a WIMP scattering is more complex than the typical WIMP-nucleon interaction, because the possible values of the momentum transfer in the interaction ( $q$ ) can be as small as  $O(100 \text{ eV})$  for WIMP masses in the MeV range and energy depositions of  $O(1-10 \text{ eV})$ , or as high as  $O(10 \text{ MeV})$  for WIMP masses in the GeV range and energy depositions of  $O(1-10 \text{ keVs})$  [29, 40].

Focusing on the direct detection of electron recoils, the velocity averaged cross section for the WIMP-electron scattering in a detector target can be determined by [18]:

$$\frac{d \langle \sigma_e v_\chi \rangle}{dE} = \frac{\bar{\sigma}_e}{2m_e} \int dv \frac{f(v_\chi)}{v_\chi} \int_{q_-}^{q_+} a_0^2 q F_\chi^2 f_{ion}(E, q) dq \quad (1)$$

where  $f(v_\chi)$  and  $v_\chi$  are the WIMP velocity distribution and WIMP velocity in the Earth frame, respectively,  $f_{ion}(E, q)$  is the ionization factor, and  $q_+$  and  $q_-$  are

the maximum and minimum momentum transfer, respectively, given by  $q_{\pm} = m_{\chi} v_{\chi} \pm \sqrt{m_{\chi}^2 v_{\chi}^2 - 2m_{\chi} E}$ , where  $m_{\chi}$  is the WIMP mass, and  $E$  is the energy deposition.

The DM form factor ( $F_{\chi}(q)$ ) and the WIMP-electron scattering cross section ( $\bar{\sigma}_e$ ) are the main expressions that contain information about the interaction mediator. These are given by [30]:

$$F_{\chi}(q) = \frac{\left(\frac{m_{DP}}{m_e}\right)^2 + \alpha^2}{\left(\frac{m_{DP}}{m_e}\right)^2 + (\alpha a_0 q)^2} \quad (2)$$

$$\bar{\sigma}_e = \frac{16 \pi a_0^2 \alpha^2 \alpha_{\chi}^2}{\left(\left(\frac{m_{DP}}{m_e}\right)^2 + \alpha^2\right)^2} \quad (3)$$

where  $\alpha$  is the fine structure constant,  $m_e$  is the electron mass,  $a_0$  is the Bohr radius, written as  $a_0 = \frac{1}{m_e \alpha}$ ,  $\alpha_{\chi}$  is the WIMP-electron coupling strength.  $\bar{\sigma}_e$  is the interaction cross section considering a free electron whose scattering with the WIMP transferred a momentum of  $a_0^{-1}$ .

Since  $\bar{\sigma}_e$  and  $F_{\chi}(q)$  depend on the mediator mass, studies usually consider two limiting cases, such that a standard scenario is established, and a precise comparison between different results becomes simple. The first case considers a heavy mediator ( $m_{DP} \gg \alpha m_e$ ), therefore,  $F_{\chi}(q) \rightarrow 1$ . The opposite case considers a light mediator ( $m_{DP} \ll \alpha m_e$ ), therefore,  $F_{\chi}(q) \rightarrow \frac{1}{(a_0 q)^2}$ .

The standard halo model has been assumed in this analysis:

$$f(v, t) \propto v^2 \exp\left(-\frac{(\vec{v} + \vec{v}_E(t))^2}{v_0^2}\right) \Theta(v - v_{esc}) \quad (4)$$

where  $\vec{v}$  is the WIMP velocity in the galactic frame,  $\vec{v}_E(t)$  is the Earth velocity in the galactic frame,  $v_0 = 220$  km/s is the Sun rotation velocity with respect to the galactic center, and  $v_{esc} = 550$  km/s is the Milky Way escape velocity.  $\vec{v}_E(t)$  depends on the relative velocity of Earth with respect to the Sun, and the peculiar velocity of the solar system in the galactic frame. This parametrization is in accordance with the procedure described in Ref. [41]. The chosen parameters values are the same considered in Ref. [30].

The raw event rate in NaI(Tl) can be determined by:

$$\frac{dR}{dE} = \frac{n_a^{NaI} \rho_{DM}}{m_{\chi}} \frac{d\langle \sigma_e v_{\chi} \rangle}{dE} \quad (5)$$

where  $n_a^{NaI}$  is the atomic number density per kilogram of NaI, and  $\rho_{DM} = 0.4$  GeV/cm<sup>3</sup> is the approximate energy

density of CDM at Earth. This  $\rho_{DM}$  value is the benchmark model for WIMP-electron scattering searches.

It is important to note that even though the number density of electrons in thallium is higher than in sodium and iodine, its concentration in COSINE-100 crystals is very low, and can be neglected in the analysis. Naive calculations have shown that the maximum contribution of thallium is about 1% of the total number of events from NaI.

Different descriptions are considered when determining the  $f_{ion}$  parameter in WIMP-electron interaction studies, and an accurate description is essential depending on the target and energies under study, as very divergent results can be obtained [42].

## B. Atomic ionization factor

The ionization factor describes the electronic structure of the target material, and different models can be considered depending on the deposited energies in the detector. The first studies conducted in xenon and argon detectors used to assume an analytic non-relativistic approach when computing  $f_{ion}$ , considering Slater-type orbitals for the bound electrons wavefunctions [18, 43]. This procedure leads to reasonable approximations when analyzing very low energy events (typically of  $O(1-10$  eV)), in which few electrons are ionized. However, it neglects important phenomena as the non-point like behavior of nuclear charge for the electron wavefunction near the nucleus, and relativistic effects, which are important for higher energy analysis. For this situation, a relativistic description of the electronic structure is important for an accurate analysis.

In this work, since the ROI is in the keV region, due to the 0.7 keV threshold of COSINE-100 crystals, sodium and iodine atoms can be considered to be free, as the typical crystal band structure energies are much lower than this [30, 44, 45]. Therefore, including the ionization factor contribution of NaI(Tl) crystal structure would marginally impact the results of this work. In general, when calculating  $f_{ion}$  for each atom isolated, it can be determined from the electron wavefunctions of each shell. However, very distinct results are obtained with different modeling of this atomic electronic structure. More details about the analytic models and a discussion and comparison between non-relativistic and relativistic methods of  $f_{ion}$  computation are presented in Appendix .

$f_{ion}$  is dependent on both  $E$  and  $q$ . Typically, for energy depositions in the keV region, there is an important contribution of  $f_{ion}$  in the range of  $q \gtrsim 1$  MeV to the event rate. For such high momentum transfer, there is a high correlation of  $f_{ion}$  with the radial electron wavefunction near the nucleus, where relativistic effects and correct nucleus size modeling are crucial. Hence, this analytical approach reproduces with good accuracy  $f_{ion}$  only for small  $q$ , which is suitable for very low energy deposition in the 1-100 eV range.

A more complete model for a keV region analysis should account for relativistic effects. A possible procedure is to numerically solve the Dirac equation, correctly considering the atomic potential for different distances of the electron from the nucleus by using the relativistic Hartree-Fock approximation [29]. This approach has been used in the DAMA/LIBRA results interpretation under the WIMP-electron scattering model. Computation of  $f_{ion}$  for sodium and iodine atoms, considering them as free, was performed by authors of the DAMA/LIBRA results interpretation study, and are publicly available in [46]. The electronic structure and methods for calculations are thoroughly discussed in [29, 30]. These results are used for the WIMP-electron interaction spectra generation in the analysis presented in this work.

A comparison between the expected spectra in NaI using the analytic non-relativistic approach, described in the Appendix, and the relativistic method for obtaining  $f_{ion}$  is presented in Fig. 3. In both cases, the iodine contribution is dominant compared to sodium, even though both are considered in this analysis.

The expected event rates below 0.4 keV are compatible for both  $f_{ion}$  models, since only low and intermediate  $q$  values (typically below 1 MeV) are dominant in this energy region. However, in the most relevant region for this analysis, above the 0.7 keV threshold, the disagreement is around one order of magnitude. Consequently, the analytic procedure underestimates the number of events, reducing the analysis sensitivity. Another notable behavior is the slight shift in ionization energies between both models. Due to the relativistic effects, electron binding energies undergo a small correction in calculations for the non-relativistic model.

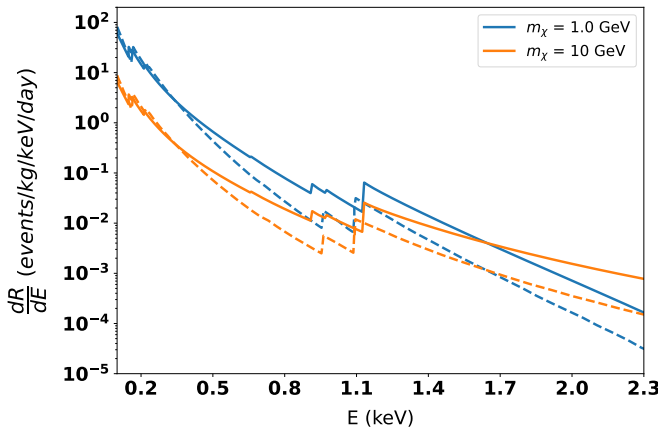


FIG. 3. Computed spectra in NaI considering the non-relativistic and relativistic methods. In the blue curves,  $m_\chi = 1$  GeV is considered, and in the orange curves,  $m_\chi = 10$  GeV is considered. Solid lines represent the computation of spectra with the relativistic approach for  $f_{ion}$  calculation, while dashed lines represent spectra with the non-relativistic approach for  $f_{ion}$  calculation.

## IV. DATA ANALYSIS

### A. Event selection

Near the 0.7 keV energy threshold, the majority of detected signals are from PMT-induced noise events, which populate both single-hit and multiple-hit crystals spectra. A single-hit event is classified when only one crystal detects two coincident signals in its PMTs, and no other hits are observed in the LS within a  $8 \mu\text{s}$  window, or other crystals within a  $4\mu\text{s}$  window. A multiple-hit event is determined when hits are observed in two or more crystals, or in the LS and in at least one crystal, satisfying the coincidence time windows mentioned above. Due to the low cross-section expected for the WIMP-electron interaction, the probability of a WIMP hitting multiple electrons is negligible. Thus, only single-hit events were considered in this analysis.

With the objective of greatly reducing the number of noise events in the ROI, a deep learning method based on the multilayer perceptron (MLP) neural network was used, allowing the reduction of analysis threshold from the previous 1 keV to 0.7 keV, maintaining an excellent event selection efficiency at the threshold level. Pulse shape discrimination likelihood parameters were introduced as inputs to MLP. The waveforms mean time and amplitudes were evaluated to obtain a PSD parameter. The fast Fourier transform of waveforms has also been included in the generation of another PSD parameter based on the waveforms power spectra. Scintillation events from calibration using the 0.87 keV X-ray emission from the electron capture process in a  $^{22}\text{Na}$  source, and noise events from PMT origin were inputs to the MLP in the sample training. A MLP score based on the likelihood parameters cited was calculated for each signal, and the event selection cut determined following the criteria that less than 1% of the selected events were noise signals [31]. The efficiency of this noise and scintillation event selection is presented and discussed in the most recent COSINE-100 WIMP-nucleon interaction search [33].

Other event selections were also applied to data in order to remove possible muon-induced events, as well as noise events originated from electronics. Regarding the latter, only events that generated at least two clusters in the waveform, and whose first trigger pulse was separated by at least  $2 \mu\text{s}$  from the beginning of the event recording were selected. Events induced by muons in the crystals were avoided by selecting only events that were not coincident with muon signals in the plastic scintillators within a 30 ms window. This is especially important, since muons might induce neutron events that deposit energies in the ROI of this analysis.

## B. COSINE-100 crystals response and WIMP-electron scattering spectra

In order to generate the expected spectra in COSINE-100 crystals for the WIMP-electron scattering model, it is essential to properly consider the detector's energy resolution and the non-linear proportionality between the measured charge in the PMTs and deposited energy at low photoelectrons level. As a consequence of the small energy deposition of WIMPs on electrons, the number of events should be higher below the 8 photoelectrons threshold. The detector performance in this region has to be rigorously studied, since these events may induce signals exceeding the threshold due to the energy resolution effect.

The crystals resolution and non-proportionality at very low energies were carefully examined by data from calibrations using the 0.87 keV X-ray emission of the  $^{22}\text{Na}$  source and background signals from the 3.2 keV X-ray peak of internal  $^{40}\text{K}$  [47]. The detector behavior has been reproduced down to one photoelectron level in the PMTs waveform simulation [48]. Accordingly to these studies, the following scaled Poisson distribution describes the crystals energy resolution for few photoelectrons yield:

$$S(q_{\text{raw}}, q_{\text{vis}}, s) = \frac{(q_{\text{raw}}/s)^{q_{\text{vis}}/s} e^{-q_{\text{raw}}/s}}{\Gamma(q_{\text{vis}}/s + 1)} \quad (6)$$

where  $q_{\text{raw}}$  is the deposited charge in the detector,  $q_{\text{vis}}$  is the visible charge, and the  $s$  parameter is determined from calibration [47].

The generated WIMP-electron spectra in COSINE-100 NaI(Tl) crystals, corrected by event selection efficiency, detectors' non-proportionality and energy resolution are presented in Fig. 4, assuming the heavy mediator scenario. Most signals are expected to be detected with energies near the 0.7 keV threshold for all WIMP masses, which makes the ROI of this analysis to be at very low energy depositions. Hence, we considered only data up to 100 photoelectrons (equivalent to about 8 keV) in the data fit. Also, the expected number of events is highest for  $m_{\chi} \approx 0.6$  GeV when considering the heavy mediator case, and for  $m_{\chi} \approx 0.2$  GeV when considering the light mediator case. Therefore, the COSINE-100 sensitivity is expected to be higher near these WIMP masses. Additionally, it is important to note that the first energy bin, for lower mass WIMPs and especially for the light mediator scenario, has multiple times the number of events of the other bins of the expected signal, making the understanding of background near the threshold very important to enhance the analysis sensitivity for WIMP masses in the MeV range.

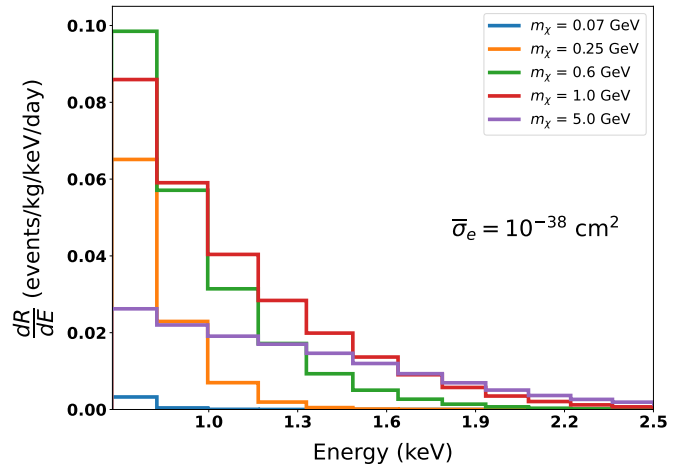


FIG. 4. Expected event rate in COSINE-100 NaI(Tl) detectors considering a heavy mediator and 5 different WIMP masses. The curves represent an average over the 5 analyzed crystals.  $\bar{\sigma}_e$  is fixed at  $10^{-38} \text{ cm}^2$ .

## C. Background components

The activities of each component that constitute the COSINE-100 crystals background are known from a detailed detector simulation based on *Geant-4* [49]. The data-set used in the background modeling is the same considered in this analysis. For energies near the 0.7 keV threshold, the dominant background components are secondary radiations from  $\beta$  decays of  $^3\text{H}$  and Compton scattered  $\gamma$ s and  $\beta$  decays of  $^{210}\text{Pb}$ , both internal sources in NaI(Tl) crystals, which represent around 75% of all events detected up to 2 keV. Fig. 5 presents the background model of COSINE-100 crystals considered in this paper.

Systematic uncertainties presented in the background model have different sources, with the most relevant at the ROI being uncertainties in the: MLP event selection efficiencies; determination of the precise location of background sources in the crystals' PMTs; evaluation of the parameters that describe the crystals' energy resolution distribution of Equation 6; non-proportionality impact on the calibration; measurement of the activity of each background component; and depth of the surface  $^{210}\text{Pb}$  in the crystals. The background model used in this analysis is the same described in the recent COSINE-100 WIMP search [33], with the only difference being that a scaled Poisson distribution is considered instead of a Gaussian distribution when correcting the spectra of background components by the energy resolution effect. This is important to match the energy resolution correction applied to the WIMP-electron interaction signals with the correction of background components spectra. The main different results to the final background model are generated by radioisotopes that produce few photoelectrons, since the shape of the scaled Poisson function differs from the

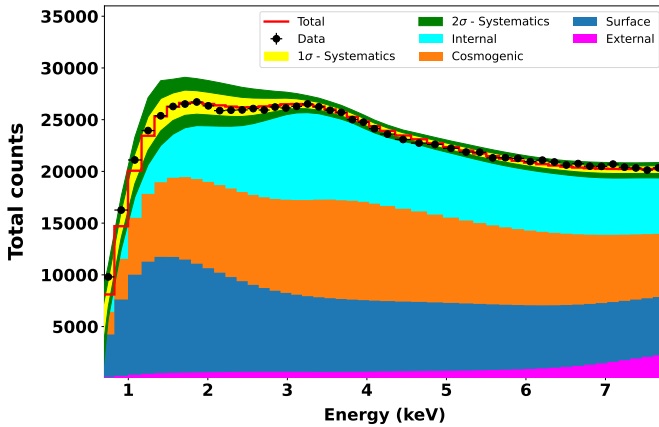


FIG. 5. Measured data for the 2.82 years data-set used in this analysis (black points), and the crystals background model in the ROI (red histogram). Data and background for all analyzed crystals are summed. Background components are labeled into 4 groups according to their origin. The yellow and green bands represent the  $1\sigma$  and  $2\sigma$  systematics, which are the dominant sources of uncertainties in the ROI.

Gaussian function at very low energy depositions. Thus,  $^{22}\text{Na}$ ,  $^{109}\text{Cd}$ , and  $^{113}\text{Sn}$  cosmogenic isotopes are the components which differed the most with the modification of energy resolution function, due to their emission of X-rays and Auger electrons near the 0.7 keV threshold. Nevertheless, when compared to the official COSINE-100 crystals background model [50], the change in the energy resolution distribution marginally increased the number of events of the background model spectrum, up to a maximum of 2% in the first energy bin.

#### D. Spectral fit

A Bayesian analysis approach was used in the spectra fit to the 2.82 years data-set process. The posterior distribution for the WIMP-electron signal was obtained from a likelihood function based on Poissonian probabilities, determined by a Markov Chain Monte Carlo (MCMC) based algorithm. This analysis method is the same adopted in other DM searches in COSINE-100 [51–54], and is thoroughly described in Ref. [55].

The fit was performed for several WIMP masses, ranging from 30 MeV to 5 GeV. The mean background activities and statistical uncertainties, determined from each crystal background model [50], were used to produce the Gaussian priors. Systematic uncertainties were included as nuisance parameters also with Gaussian priors. Each crystal background is allowed to independently fluctuate in the simultaneous fit performed, but the  $\bar{\sigma}_e$  distribution is marginalized over all 5 crystals. No evidence of excess events consistent with expected spectra from both the light and heavy mediator models was found. The resulting fit for a 0.6 GeV WIMP and assuming a heavy mediator is presented in Fig. 6, along with the expected

observed data for  $\bar{\sigma}_e = 9.2 \times 10^{-38} \text{ cm}^2$ .

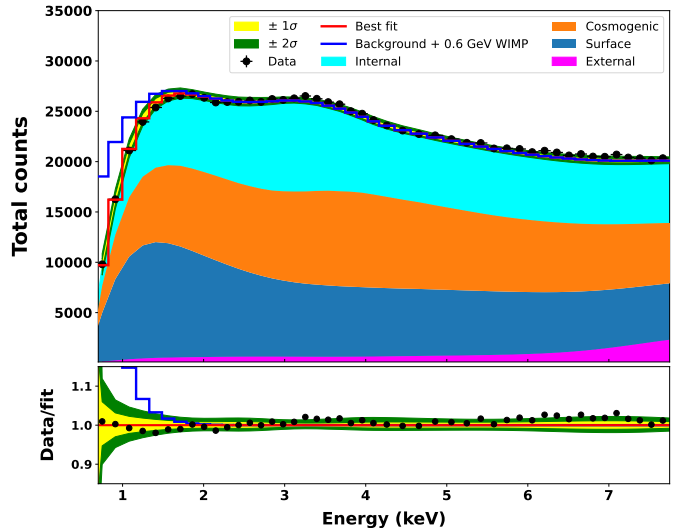


FIG. 6. COSINE-100 data fit results for  $m_\chi = 0.6$  GeV, assuming the heavy mediator scenario. Background components, separated into their different origins, are presented. Yellow and green bands represent the  $1\sigma$  and  $2\sigma$  fit uncertainties, respectively. The expected measured data for the WIMP-electron cross section of  $\bar{\sigma}_e = 9.2 \times 10^{-38} \text{ cm}^2$  that best fits DAMA/LIBRA modulation, presented in Ref. [30], is also shown in the blue histogram.

After marginalization, the resulting posterior probability distribution function (PDF) for the WIMP-electron signal strength is used to set a 90% confidence level (CL) upper limits on  $\bar{\sigma}_e$ . Fig. 7 shows the posterior distribution for the 0.6 GeV WIMP data fit.

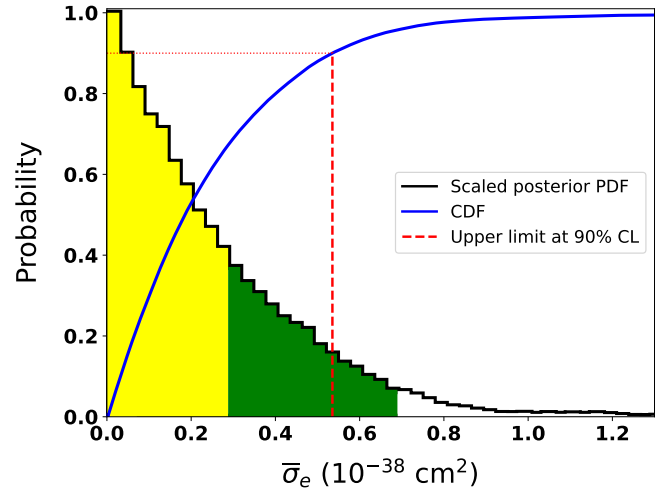


FIG. 7. Normalized posterior distribution for  $\bar{\sigma}_e$ , considering a  $m_\chi = 0.6$  GeV WIMP and a heavy mediator. Yellow and green bands represent the  $1\sigma$  and  $2\sigma$  CL probabilities, respectively. The blue curve shows the cumulative distribution function (CDF).

Simulated data samples based on the background model were produced in order to test the analysis sensitivity. Based on the Gaussian priors of each crystal background component and systematic uncertainties, 1000 pseudo-data samples were generated assuming a background-only hypothesis. The same fitting procedure of the physics data was used, and 90% CL upper limits were set for each sample. The resulting upper limits distribution for each WIMP mass was used to perform calculations of the mean sensitivity and its  $1\sigma$  and  $2\sigma$  uncertainty bands. Fig. 8 presents the limits set for light and heavy mediator models.

In the light mediator scenario, the distance between the set upper limits and the median sensitivity remains almost constant for any WIMP mass. This effect reflects the small change in the spectra shape for low WIMP masses, and particularly for the light mediator model, a spectrum shape variation is only relevant above 10 GeV.

The upper limits set from this COSINE-100 data analysis for a light and heavy mediator scenarios do not explore regions unconstrained by the most sensitive experiments for the WIMP-electron interaction model, due to their capability of reaching very low threshold (down to a single electron ionization [17]). However, the reported COSINE-100 constraints completely exclude the best fit regions for the DAMA/LIBRA modulation results assuming any vector mediator mass, and set the current most stringent upper limits for the WIMP-electron scattering model for a NaI(Tl) experiment.

## V. PROSPECTS FOR COSINE-100 AND COSINE-100U

The COSINE-100U experiment will be the upgraded version of COSINE-100 [56]. It will be located at the *Yemilab* underground laboratory, also in South Korea. The new laboratory is 300 m deeper than *Yang Yang*, reducing even more the contribution of cosmic rays in the experiment. The main objective of COSINE-100U is to enhance the NaI(Tl) crystals light yield and make all 8 crystals suitable for low energy analysis, reducing the detector threshold, and increasing sensitivity to sub-GeV DM searches.

A new encapsulation method, focused on removing the need for a quartz light guide between the crystals' end faces and PMTs, has been proved to reduce scintillation photon losses and improve light collection [57, 58]. The crystals operation at  $-30^{\circ}\text{C}$  also provides an increase in light yield [59]. Both upgrades will be applied to COSINE-100U experiment, and are expected to enhance light yield by about 40%. This is expected to enable a reduction of the analysis threshold from 8 photoelectrons to 5 photoelectrons.

Since the expected number of events for the WIMP-electron interaction in NaI(Tl) is much higher for very low energy depositions, as presented in the spectra of Fig. 4, a threshold reduction of the crystals would remarkably

enhance the analysis sensitivity. Fig. 9 shows an estimated projection of the constraints for COSINE-100U, assuming a 5 photoelectrons threshold. The prospects indicate a notable improvement in sensitivity for low mass WIMPs, however, it remains uncompetitive with limits established by other experiments.

An analysis below the current 0.7 keV COSINE-100 threshold, potentially extended down to a one photoelectron level, is currently being investigated. Given that a precise background modeling at such a small energy deposition is unfeasible due to the very high noise rate, an alternative approach in terms of event selection and data analysis will be required. It is proposed to conduct an annual modulation analysis, which is less reliant on the exact determination of background activity, provided that the stability of noise and background rates are ensured. Once the feasibility of this study is confirmed using COSINE-100 data, it can be implemented in COSINE-100U NaI(Tl) crystals to enhance the analysis sensitivity due to the higher light emission and collection efficiency.

To accurately assess WIMP-electron scattering events that deposit energies below the keV region, it is no longer appropriate to treat sodium and iodine atoms as free within COSINE-100 crystals, as the NaI(Tl) crystal band structure becomes relevant. Studies on the behavior of the NaI(Tl) crystal at low energy depositions have shown promising results of this material when compared to silicon, xenon and argon, which compose the most sensitive experiments to WIMP-electron search [44, 60].

## VI. CONCLUSION

We reported the search for WIMP scattering on electrons using a 2.82 years data-set of the COSINE-100 experiment NaI(Tl) crystals. We found no excess events consistent with the expected signals for the WIMP-electron interaction assuming a heavy or a light vector boson mediator. 90% confidence level upper limits were set on the WIMP-electron scattering cross section. The most stringent constraints exclude cross sections above  $6.4 \times 10^{-33} \text{ cm}^2$  for a 0.25 GeV WIMP, assuming a light mediator, and above  $3.4 \times 10^{-37} \text{ cm}^2$  for a 0.4 GeV WIMP, assuming a heavy mediator. These results represent the most restrictive exclusion limits on the WIMP-electron scattering model for a NaI(Tl) target to date, and fully cover the parameters attributed to DAMA/LIBRA modulation results interpreted within this framework. We propose a more sensitive analysis in NaI(Tl) crystals, aiming the investigation of events that generate few photoelectrons in the PMTs. This study could potentially allow the search for MeV WIMPs in NaI(Tl), and will be the subject of a future report.

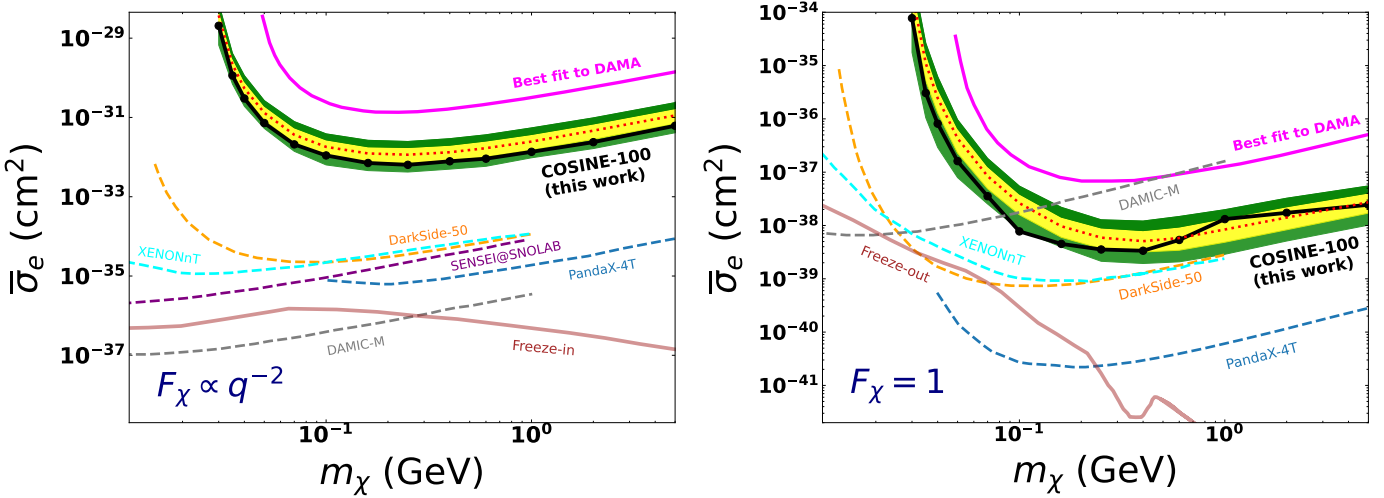


FIG. 8. Upper limits for  $\bar{\sigma}_e$  considering the light mediator model (left) and heavy mediator model (right). The dotted red lines and the yellow and green areas represent the median 90 % CL expected sensitivity and its  $1\sigma$  and  $2\sigma$  bands, respectively. The magenta lines are the best fit to DAMA/LIBRA modulation results, presented in Ref. [30]. Constraints from the PandaX-4T [23], SENSEI [22], DarkSide-50 [24], XENONnT [25] and DAMIC-M [21] experiments are also shown. The brown shaded regions show required parameters from models which obtain the observed DM relic abundance by freeze-in (light mediator) or freeze-out (heavy mediator) mechanisms [16].

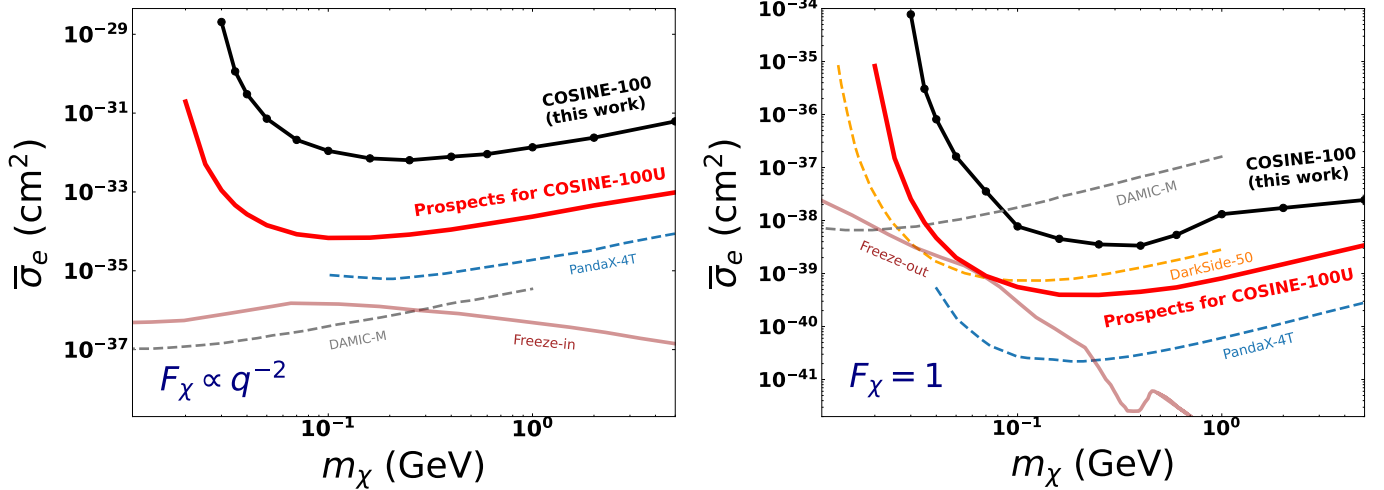


FIG. 9. Sensitivity prospects for the COSINE-100U experiment (red) considering the light mediator model (left) and heavy mediator model (right), for 90% CL. The black data points represent the upper limits set for COSINE-100 in this study. The most stringent constraints from experiments and the models parameters for freeze-in and freeze-out are also shown.

## ACKNOWLEDGMENTS

We thank the Korea Hydro and Nuclear Power (KHNP) Company for providing underground laboratory space at Yangyang and the IBS Research Solution Center (RSC) for providing high performance computing resources. This work is supported by: the Institute for Basic Science (IBS) under project code IBS-R016-A1, NRF-2021R1A2C3010989, NRF-2021R1A2C1013761, RS-2024-00356960, RS-2025-25442707 and RS-2025-16064659, Republic of Ko-

rea; NSF Grants No. PHY-1913742, United States; STFC Grant ST/N000277/1 and ST/K001337/1, United Kingdom; Grant No. 2021/06743-1, 2022/12002-7, 2022/13293-5 and 2025/01639-2 FAPESP, CAPES Finance Code 001, CNPq 304658/2023-5, Brazil; LPDP Grant under WCU Equity 2024, Indonesia.

## Appendix: Non-relativistic $f_{ion}$ calculation, and comparison with relativistic model

The analytic calculation method for  $f_{ion}$  considered in the non-relativistic spectra presented in Fig. 3 is the same used in the studies reported by DarkSide-50 collaboration [24, 43]. The Roothan-Hartree-Fock (RHF) wavefunctions represent the radial part of bound electrons. These are written as a linear combination of hydrogen-like wavefunctions (Slater-type orbitals) [61].

For ionized electrons, the radial wavefunctions are obtained from the solution to the Schrödinger equation with the Coulomb potential  $-Z_{eff}^{nl}/r$ , where  $Z_{eff}^{nl}$  is the effective charge observed by the scattered electron, and  $n$  and  $l$  indicate the electron shell. This charge is determined in order to reproduce the binding energy of the electron, assuming only the effect of a Coulomb potential.

Near the nucleus (electron wavefunction for  $r \ll R$ , where  $R$  is the atom radius),  $Z_{eff}^{nl}$  is expected to tend to  $Z$ , since only the nuclear charge becomes relevant. The opposite happens far from the nucleus (electron wavefunction for  $r \gg R$ ), where  $Z_{eff}^{nl}$  should tend to 1, as the total charge of the ionized atom becomes unity. This process is not accounted for when defining a fixed value for  $Z_{eff}^{nl}$  from the Coulomb potential as described.

It is possible to insert into the analytic model an effective charge dependent on the distance between the electron and the nucleus, derived from the "frozen core approximation" [62]. In this formulation,  $Z_{eff}^{nl}(r)$  can be written by:

$$Z_{eff}^{nl}(r) = Z + \nu_{nl}(r) - \sum_b (2j_b + 1) \nu_b(r) \quad (\text{A.1})$$

where the sum over  $b$  is over all bound electrons, and  $2j_b + 1$  is the number of bound electrons in shell  $b = l$ .  $\nu(r)$  is the potential of a single electron, which is obtained from the radial components of electron wavefunctions of each shell by:

$$\nu_{nl}(r) = \int_0^\infty dr' r'^2 \frac{R_{nl}^2(r)}{r'} \quad (\text{A.2})$$

where  $r_>$  is the highest value between  $r$  and  $r'$ .

In contrast to the case of a fixed  $Z_{eff}^{nl}$ , the effective charge of the ionized electron varies with  $r$ . Furthermore, there is no significant difference in the dependence

of  $Z_{eff}^{nl}$  on  $r$  for electrons from any shell, given that the effective charge is barely sensitive to the ground state electron shell. Fig. 10 shows the comparison between  $f_{ion}$  calculated according to the analytic method assuming a fixed  $Z_{eff}^{nl}$ , a  $Z_{eff}^{nl}(r)$  (dependent on  $r$ ), and according to the relativistic method. Calculations were performed for Na and I atoms considering a 2 keV energy deposition. For this energy deposition, the iodine electrons of the 1s, 2s, and 2p shells do not contribute to  $f_{ion}$ , since their binding energies are higher than the deposited energy.

Despite resulting in a reasonable description of  $f_{ion}$  for intermediate values of  $q$  (generally in the 100 keV to 1 MeV range), this non-relativistic approach fails to accurately describe the electron scattering behavior for small and high momentum transfers.

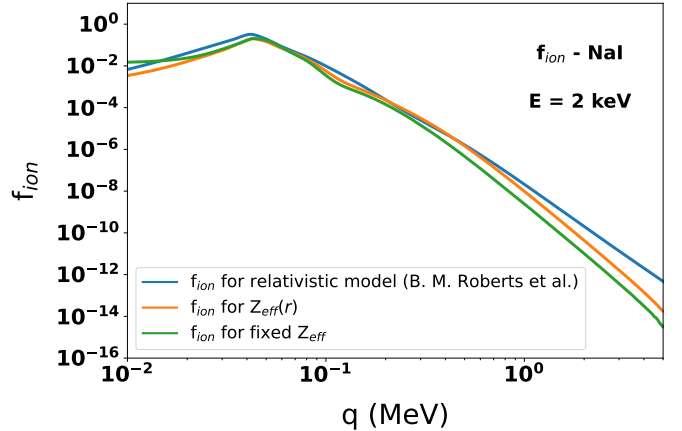


FIG. 10. Comparison between different methods for performing the  $f_{ion}$  calculation for NaI, considering a 2 keV energy deposition. The  $f_{ion}$  calculated by the relativistic method [42, 46], by the  $Z_{eff}^{nl}$  dependent on  $r$  model, and by the fixed  $Z_{eff}^{nl}$  model are presented by the blue, orange and green curves, respectively.

Updating the non-relativistic model with a  $Z_{eff}^{nl}$  dependent on  $r$  is able to make  $f_{ion}$  more compatible with the relativistic approach, particularly at intermediate  $q$ . However, it still lacks a correct modeling of electron wavefunctions near the nucleus, whose contribution is dominant for large  $q$ . Having in mind that for energy deposition in the keV range  $q$  can be up to 50 MeV for  $m_\chi$  in the GeVs, it is exceptionally important to include relativistic effects in the  $f_{ion}$  computation of this COSINE-100 data analysis of the WIMP-electron scattering model.

---

[1] K. Freese, *EAS Publ. Ser.* **36**, 113 (2009), [arXiv:0812.4005 \[astro-ph\]](https://arxiv.org/abs/0812.4005).

[2] T. M. C. Abbott *et al.* (DES Collaboration), *The Astrophysical Journal Letters* **872**, L30 (2019).

[3] J. R. Bond, J. Centrella, A. S. Szalay, and J. R. Wilson, "Dark matter shocked pancakes," in *Formation and Evolution of Galaxies and Large Structures in the Universe*, edited by J. Audouze and J. Tran Thanh Van (Springer Netherlands, Dordrecht, 1984) pp. 87–99.

[4] S. Colombi, S. Dodelson, and L. M. Widrow, *Astrophys. J.* **458**, 1 (1996), [arXiv:astro-ph/9505029 \[astro-ph\]](https://arxiv.org/abs/astro-ph/9505029).

[5] G. Bertone and T. M. P. Tait, *Nature* **562**, 51 (2018).

[6] J. L. Feng, *SciPost Phys. Lect. Notes* , **71** (2023).

[7] G. Jungman, M. Kamionkowski, and K. Griest, *Physics Reports* **267**, 195 (1996).

[8] A. H. Abdelhameed *et al.* (CRESST Collaboration), *Phys. Rev. D* **100**, 102002 (2019).

[9] P. Agnes *et al.* (DarkSide-50 Collaboration), *Phys. Rev. D* **107**, 063001 (2023).

[10] J. Aalbers *et al.* (LUX-ZEPLIN Collaboration), *Phys. Rev. Lett.* **131**, 041002 (2023).

[11] E. Aprile *et al.* (XENON Collaboration), *Phys. Rev. Lett.* **123**, 241803 (2019).

[12] L. Necib, J. Moon, T. Wongjirad, and J. M. Conrad, *Phys. Rev. D* **95**, 075018 (2017).

[13] K. Sigurdson, M. Doran, A. Kurylov, R. R. Caldwell, and M. Kamionkowski, *Phys. Rev. D* **70**, 083501 (2004).

[14] M. Fabbrichesi, E. Gabrielli, and G. Lanfranchi, *The physics of the dark photon* (Springer International Publishing, 2021).

[15] R. D. Peccei, “The strong cp problem and axions,” in *Axions: Theory, Cosmology, and Experimental Searches*, edited by M. Kuster, G. Raffelt, and B. Beltrán (Springer Berlin Heidelberg, Berlin, Heidelberg, 2008) pp. 3–17.

[16] R. Essig, M. Fernández-Serra, J. Mardon, A. Soto, T. Volansky, and T.-T. Yu, *Journal of High Energy Physics* **2016**, 46 (2016).

[17] E. Aprile *et al.* (XENON Collaboration), *Phys. Rev. D* **106**, 022001 (2022).

[18] R. Essig, A. Manalaysay, J. Mardon, P. Sorensen, and T. Volansky, *Phys. Rev. Lett.* **109**, 021301 (2012).

[19] Z. Y. Zhang *et al.* (CDEX Collaboration), *Phys. Rev. Lett.* **129**, 221301 (2022).

[20] Q. Arnaud *et al.* (EDELWEISS Collaboration), *Phys. Rev. Lett.* **125**, 141301 (2020).

[21] K. Aggarwal *et al.* (DAMIC-M Collaboration), *Phys. Rev. Lett.* **135**, 071002 (2025).

[22] P. Adari *et al.* (SENSEI Collaboration), *Phys. Rev. Lett.* **134**, 011804 (2025).

[23] S. Li *et al.* (PandaX Collaboration), *Phys. Rev. Lett.* **130**, 261001 (2023).

[24] P. Agnes *et al.* (DarkSide Collaboration), *Phys. Rev. Lett.* **130**, 101002 (2023).

[25] E. Aprile *et al.* (XENON Collaboration), *Phys. Rev. Lett.* **134**, 161004 (2025).

[26] J. J. Choi *et al.* (NEON Collaboration), *Phys. Rev. Lett.* **134**, 021802 (2025).

[27] R. Bernabei, P. Belli, A. Bussolotti, F. Cappella, V. Caracciolo, R. Cerulli, C. Dai, A. d’Angelo, A. Di Marco, H. He, *et al.*, *Nuclear and Particle Physics Proceedings* **303-305**, 74 (2018), 7th Workshop on Theory, Phenomenology and Experiments in Flavour Physics.

[28] R. Bernabei, P. Belli, A. Bussolotti, F. Cappella, V. Caracciolo, R. Cerulli, C. Dai, A. d’Angelo, N. Ferrari, A. Incicchitti, *et al.*, *Nuclear Physics and Atomic Energy* **22**, 329 (2021).

[29] B. M. Roberts, V. A. Dzuba, V. V. Flambaum, M. Pospelov, and Y. V. Stadnik, *Phys. Rev. D* **93**, 115037 (2016).

[30] B. M. Roberts and V. V. Flambaum, *Phys. Rev. D* **100**, 063017 (2019).

[31] G. H. Yu *et al.* (COSINE-100 Collaboration), *Journal of Instrumentation* **19**, P12013 (2024).

[32] N. Carlin *et al.* (COSINE-100 Collaboration), *Science Advances* **11**, eadv6503 (2025).

[33] G. H. Yu *et al.* (COSINE-100 Collaboration), *arXiv:2501.13665 [hep-ex]*.

[34] “Grafana Application,” <https://grafana.com>.

[35] G. Adhikari, P. Adhikari, E. B. de Souza, N. Carlin, S. Choi, W. Q. Choi, M. Djamel, A. C. Ezeribe, C. Ha, I. S. Hahn, *et al.*, *The European Physical Journal C* **78**, 107 (2018).

[36] G. Adhikari *et al.* (COSINE-100 Collaboration), *Nuclear Instruments and Methods in Physics Research Section A: Accelerators, Spectrometers, Detectors and Associated Equipment* **1006**, 165431 (2021).

[37] H. Prihtiadi *et al.* (COSINE-100 Collaboration), *Journal of Instrumentation* **13**, T02007 (2018).

[38] G. Adhikari *et al.* (COSINE-100 Collaboration), *Journal of Instrumentation* **17**, T01001 (2022).

[39] J. Engel, S. Pittel, and P. Vogel, *International Journal of Modern Physics E* **01**, 1 (1992), <https://doi.org/10.1142/S0218301392000023>.

[40] S. K. Lee, M. Lisanti, S. Mishra-Sharma, and B. R. Safdi, *Phys. Rev. D* **92**, 083517 (2015).

[41] K. Freese, M. Lisanti, and C. Savage, *Rev. Mod. Phys.* **85**, 1561 (2013).

[42] A. R. Caddell, V. V. Flambaum, and B. M. Roberts, *Phys. Rev. D* **108**, 083030 (2023).

[43] P. Agnes *et al.* (The DarkSide Collaboration), *Phys. Rev. Lett.* **121**, 111303 (2018).

[44] S. Derenzo, R. Essig, A. Massari, A. Soto, and T.-T. Yu, *Phys. Rev. D* **96**, 016026 (2017).

[45] S. M. Griffin, K. Inzani, T. Trickle, Z. Zhang, and K. M. Zurek, *Phys. Rev. D* **104**, 095015 (2021).

[46] B. Roberts and A. Caddell, “Atomicionisation,” <https://github.com/benroberts999/AtomicIonisation> (2023).

[47] S. M. Lee *et al.* (COSINE-100 Collaboration), *The European Physical Journal C* **84**, 484 (2024).

[48] J. Choi, C. Ha, E. Jeon, K. Kim, S. Kim, Y. Kim, Y. Ko, B. Koh, H. Lee, S. Lee, *et al.*, *Nuclear Instruments and Methods in Physics Research Section A: Accelerators, Spectrometers, Detectors and Associated Equipment* **1065**, 169489 (2024).

[49] S. Agostinelli, J. Allison, K. Amako, J. Apostolakis, H. Araujo, P. Arce, M. Asai, D. Axen, S. Banerjee, G. Barrand, *et al.*, *Nuclear Instruments and Methods in Physics Research Section A: Accelerators, Spectrometers, Detectors and Associated Equipment* **506**, 250 (2003).

[50] G. H. Yu *et al.* (COSINE-100 Collaboration), *The European Physical Journal C* **85**, 32 (2025).

[51] G. Adhikari *et al.* (COSINE-100 Collaboration), *Phys. Rev. Lett.* **131**, 201802 (2023).

[52] G. Adhikari *et al.* (COSINE-100 Collaboration), *Phys. Rev. D* **108**, 092006 (2023).

[53] G. Adhikari *et al.* (COSINE-100 Collaboration), *Phys. Rev. D* **108**, L041301 (2023).

[54] P. Adhikari *et al.* (COSINE-100 Collaboration), *Astroparticle Physics* **114**, 101 (2020).

[55] G. Adhikari *et al.* (COSINE-100 Collaboration), *Science Advances* **7**, eabk2699 (2021).

[56] D. Lee, J. Y. Cho, C. H. Ha, E. Jeon, H. Kim, J. Kim, K. Kim, S. Kim, S. K. Kim, W. K. Kim, *et al.*, *Communications Physics* **8**, 135 (2025).

[57] J. Choi, B. Park, C. Ha, K. Kim, S. Kim, Y. Kim, Y. Ko, H. Lee, S. Lee, and S. Olsen, *Nuclear Instruments and Methods in Physics Research Section A: Accelerators, Spectrometers, Detectors and Associated Equipment*

ment **981**, 164556 (2020).

[58] J. Choi *et al.* (NEON Collaboration), *Journal of Instrumentation* **19**, P10020 (2024).

[59] S. Lee, G. Kim, H. Kim, K. Kim, J. Lee, and H. Lee, *Astroparticle Physics* **141**, 102709 (2022).

[60] T. D. Trickle, *Direct Detection of Light Dark Matter with Electrons, Phonons, and Magnons*, Ph.D. thesis, Caltech (2022).

[61] A. McLean and R. McLean, *Atomic Data and Nuclear Data Tables* **26**, 197 (1981).

[62] M. K. Pandey, L. Singh, C.-P. Wu, J.-W. Chen, H.-C. Chi, C.-C. Hsieh, C.-P. Liu, and H. T. Wong, *Phys. Rev. D* **102**, 123025 (2020).